Revista Brasileira de Cartografia (2014) N⁰ 66/7 - International Issue: 1437-1449
Sociedade Brasileira de Cartografia, Geodésia, Fotogrametria e Sensoriamento Remoto
ISSN: 1808-0936

SUNGLINT CORRECTION IN AIRBORNE HYPERSPECTRAL IMAGES OVER INLAND WATERS

Correção dos Efeitos de "sunglint" em Imagens Hiperespectrais Aerotransportadas em Águas Interiores

Annia Susin Streher[1], Cláudio Clemente Faria Barbosa[1], Lênio Soares Galvão[2], James A. Goodman[3], Thiago Sanna Freira Silva[2] & Evlyn Márcia Leão Moraes Novo[2]

[1]Instituto Nacional de Pesquisas Espaciais – INPE
Divisão de Processamento de Imagens – DPI
Caixa Postal 515, 12245-970, São José dos Campos, SP, Brazil
annia@dpi.inpe.br ,claudio@dpi.inpe.br;

[2]Instituto Nacional de Pesquisas Espaciais – INPE
Divisão de Sensoriamento Remoto – DSR
Caixa Postal 515, 12245-970, São José dos Campos, SP, Brazil.
lenio@dsr.inpe.br , thiago@dsr.inpe.br , evlyn@dsr.inpe.br

[3] HySpeed Computing
PO Box 431824, Miami, FL 33243, USA
jgoodman@hyspeedcomputing.com

Recebido em 25 de Abril, 2014/ Aceito em 19 de Junho, 2014
Received on April 25, 2014/ Accepted on Juny 19, 2014

ABSTRACT

This study assessed sunglint effects, also known as the specular reflection from the water surface, in high-spatial and high-spectral resolution, airborne images acquired by the SpecTIR sensor under different view-illumination geometries over the Brazilian Ibitinga reservoir (Case II waters). These effects were corrected using the Goodman et al. (2008) and the Kutser et al. (2009) methods, and a Kutser et al. (2009) variant based on the continuum removal technique to calculate the oxygen absorption band depth. The performance of each method for reducing sunglint effects was evaluated by a quantitative analysis of pre- and post-sunglint correction reflectance values (residual reflectance images). Furthermore, the analysis was supported by inspection of the reflectance differences along transects placed over homogeneous masses of waters and over specific portions of the scenes affected and non-affected by sunglint. Results showed that the algorithm of Goodman et al. (2008) produced better results than the other two methods, as it approached zero amplitude reflectance values between homogenous water masses affected and non-affected by sunglint. The Kutser et al. (2009) method also presented good performance, except for the most contaminated sunglint portions of the scenes. When the continuum removal technique was incorporated to the Kutser et al. (2009) method, results varied with the scene and were more sensitive to atmospheric correction artifacts and instrument signal-to-noise ratio characteristics.

Keywords: Hyperspectral Remote Sensing, Specular Reflection, Water Optically Active Substances, SpecTIR Sensor.

RESUMO

Este estudo avaliou os efeitos de sunglint, também conhecido como reflexão especular da água, em imagens hiperespectrais de alta resolução espacial adquiridas pelo sensor aerotransportado SpecTIR sob diferentes geometrias de iluminação e de visada no reservatório de Ibitinga, SP (águas do caso II). Estes efeitos foram corrigidos usando os métodos de Goodman et al. (2008) e Kutser et al. (2009), além de uma adaptação deste último, a qual foi baseada na técnica de remoção do contínuo para calcular a profundidade da banda de absorção de oxigênio. O desempenho de cada método na remoção dos efeitos de sunglint foi avaliada por uma análise quantitativa dos valores de reflectância pré e pós-correção (imagens de reflectância residuais). A análise foi corroborada pela inspeção das diferenças na reflectância ao longo de transectos sobre massas homogêneas de águas ou sobre partes específicas das cenas afetadas e não afetadas por sunglint. Os resultados mostraram que o algoritmo de Goodman et al. (2008) produziu resultados melhores do que os outros dois métodos, uma vez que a amplitude dos valores de reflectância entre massas de água homogêneas livres e contaminadas por sunglint aproximaram-se de zero. O método de Kutser et al. (2009) também obteve bom desempenho, exceto para as partes mais contaminadas das cenas. Ao incorporar a técnica de remoção do contínuo ao método de Kutser et al. (2009), os resultados variaram de acordo com a cena e foram mais sensíveis aos artefatos de correção atmosférica e a relação sinal-ruído.

Palavras chaves: Sensoriamento Remoto Hiperspectral, Reflexão Especular, Constituintes Opticamente Ativos da água, Sensor SpecTIR.

1. INTRODUCTION

Optical remote sensing plays an important role in improving our understanding on the dynamics of Earth's inland waters due to the ability of many instruments to collect data over large areas at different times of the year. Actually, optical remote sensing includes a broad range of applications such as water quality assessment (KOPONEN et al., 2002; KEITH et al., 2012); determination of pigment content (GURLIN et al, 2011; MOSES et al., 2012); estimation of total suspended solids concentration (OLMANSON et al., 2013); classification of benthic habitats (BERTELS et al., 2008; KUTSER et al., 2009; SILVA et al., 2008; CASAL et al., 2011); and bathymetry retrieval (GOODMAN et al., 2008).

However, many inland water bodies often have spatial extents that are smaller than the resolving power of many satellite sensors. In this case, airborne imaging offers the advantage of increased control over the data collection process, making it more suitable for assessing the spatial and temporal dynamics of these smaller inland water environments. Furthermore, airborne imaging spectrometers can be utilized to acquire data with finer spectral resolution than that available in orbital sensors, allowing better detection, estimation and classification of most water constituents, such as photosynthesizing pigments, which are a key component of Case II waters (MOSES et al., 2012; KUTSER et al., 2006).

Case II waters are considered an optically complex type of water, characterized by high concentrations of suspended sediments and colored dissolved organic matter (CDOM), which mask phytoplankton scattering response. In Case I waters, phytoplankton organisms are primarily responsible for the variations in the water optical properties (MOREL & PRIEUR, 1977). According to ODERMATT et al. (2012), spectral variation within case II waters is large, because concentrations as well as specific inherent optical properties of chlorophyll (CHL), total suspended matter (TSM) and colored dissolved organic matter (CDOM) are subject to potentially large and independent variability. Airborne imaging spectrometers therefore provide both spatial and spectral advantages that can be specifically adjusted on a per study basis to allow adequate coverage of a given study area and application objective (MOSES et al., 2012; BERTELS et al., 2008).

Both orbital and airborne optical sensors can be heavily affected by the occurrence of sunglint, which occurs when the water surface orientation is such that sun light is directly reflected towards the sensor (KAY et al., 2009). This reflected radiation adds a component to the registered signal that does not carry any information about the water volume and which can be much higher than the water leaving signal in all spectral bands. In many cases, the sunglint signal saturates pixel values

and completely obscures the information of chlorophyll concentration and other optically active substances (OAS), requiring higher radiometric sensitivities to properly register useful information (KAY et al., 2009).

The occurrence and intensity of sunglint is a function of water surface roughness, sun position and viewing geometry (KAY et al., 2009; KUTSER et al., 2013). In airborne campaigns, sunglint effects can be minimized by optimizing flight paths, such as having the sensor flown toward or away from the Sun (MUSTARD et al., 2001), and by keeping solar zenith angles between 30° and 60° (DEKKER et al., 2001). However, these directives cannot always be enforced due to the variable size and spatial configuration of the water bodies. Sinuous and irregular meandering rivers and reservoirs can be particularly challenging when planning airborne image acquisition as different acquisition geometries are needed to cover the entire area. In these cases, sunglint effects may become a serious limitation for accurately determining water optical characteristics from remotely sensed data, requiring specific methods to reduce or compensate its effects on the images (MUSTARD et al., 2001; KAY et al., 2009).

Most sunglint removal algorithms developed for high spatial resolution images use the spectral response from near infrared (NIR) bands to estimate the amount of sunglint in each pixel (KAY et al., 2009; CASAL et al., 2011). These algorithms assume that the water leaving signal is negligible in this spectral region, and that any remaining signal after atmospheric correction is caused by sunglint. Under this assumption, the spectrum from the deepest regions of the water body (i.e. highest absorption in the NIR range) is used to define a linear relationship between NIR reflectance and sunglint reflectance in the visible (VIS) region (HOCHBERG et al., 2003; HEDLEY et al., 2005; LYZENGA et al., 2006). This relationship has its physical basis on the water refraction index, which is nearly the same for both VIS and NIR wavelengths (MOBLEY, 1994). It is possible to assume that changes in the intensity and anisotropy of the underwater light field related to Sun´s position (VOSS & MOREL, 2005) can be neglected due to the overwhelming intensity of the specular component. However, it is not always possible to assume that NIR reflectance is negligible, as it may be affected by bottom reflectance, concentration of inorganic particles, and phytoplankton scattering. For example, the methods developed by HOCHBERG et al. (2003) and HEDLEY et al. (2005) overcorrect the sunglint signal in shallow and/or high turbidity waters (GOODMAN et al., 2008; KUTSER et al., 2009; KAY et al., 2009). Furthermore, these methods were developed for multispectral images, and are not necessarily adaptable to operational use with hyperspectral data (MILLER, 2012).

Alternative methods for hyperspectral images have been suggested by GOODMAN et al. (2008) and KUTSER et al. (2009). The method by GOODMAN et al. (2008) is based on the radiative transfer model from LEE et al. (1999). In this method, NIR radiance is subtracted from the radiance at each wavelength, and a constant offset is added as a function of the magnitude of reflectance at 640 nm. This method is advantageous because it allows sunglint correction under cross-scene variation, as each pixel is corrected independently (KAY et al., 2009). In contrast, the KUTSER et al. (2009) algorithm is based on the 763 nm oxygen absorption band. If atmosphere correction is effective, reflectance in this wavelength should be zero in the deepest portions of the water bodies. Any remaining signal can be then attributed to sunglint effects.

The objective of this study was to assess the performance of three sunglint removal methods applied to hyperspectral imagery acquired by the airborne SpecTIR sensor under different view-illumination geometries. The following methods were tested: GOODMAN et al. (2008), KUTSER et al. (2009) and a variant of the KUTSER et al. (2009) method that included the continuum removal approach (CLARK & ROUSH, 1984) to calculate the oxygen absorption band depth.

2. METHODS

The approach was based on the use of seven hyperspectral images acquired using the SpecTIR airborne sensor. Three different algorithms were utilized to minimize sunglint effects in these images, which each contained varying sunglint intensities. This section describes image acquisition and pre-processing,

the algorithms used to remove sunglint effects, and the methodology used to evaluate algorithm performance.

2.1 Study area

The Ibitinga reservoir is located in the state of São Paulo (Southeastern Brazil) as part of the Tietê River basin (Fig. 1). Ibitinga has an area of 114 km^2, a perimeter of 450 km (CESP, 1998) and approximate major axis of 70 km along the Tietê River, while also extending 25 km along the Jacaré-Guaçu River and 25 km along the Jacaré-Pepira River. The average water volume is approximately 56 x 106 m^3, with an average depth of 9 m and a water residence time of 22 days (CESP, 1998).

2.2 Hyperspectral image acquisition and processing

Seven images were acquired over Ibitinga reservoir on October 24, 2011, using the SpecTIR hyperspectral airborne sensor (SpecTIR, LLC), operated by the FotoTerra company (http://www.fototerra.com.br). This imaging spectrometer obtains images in 357 bands positioned in the VIS, NIR and shortwave infrared (SWIR) (398-2455 nm), with a bandwidth of 5 nm. SpecTIR has a 24° field-of-view (FOV) and a 0.075° instantaneous field-of-view (IFOV). The radiometric resolution is 16 bits and the SNR is 500:1 (VIS-NIR), making this sensor well suited for the assessment of optically complex and highly dynamic inland water bodies. In the present study, only the noise-free SpecTIR bands located between 430 nm and 1000 nm were used. Images were acquired at nadir viewing and the spatial resolution was 3 meters.

Ibitinga reservoir has a meandering shape, which demanded constant changes in data acquisition geometry to achieve adequate areal coverage. View-illumination parameters for each one of the seven flight lines are shown in Table 1.

Atmospheric correction and the conversion from radiance data into surface reflectance images were performed using the Fast Line-of-Sight Atmospheric Analysis of Spectral Hypercubes (FLAASH) algorithm, a MODTRAN4-based approach to remove atmospheric scattering and absorption effects (FELDE et al., 2003; ITT, 2005). A tropical atmosphere model and rural particle model for aerosol type were selected. Water vapor content was estimated on a per-pixel basis using the 1135-nm spectral feature. The visibility was set up to 70 km for all scenes.

Geometric correction was also performed for each reflectance image using the Map Tools package in the Environment for Visualizing Images (ENVI 4.8) (ITT, 2005). The Geometry Look-up Table (GLT) data for each flight line, which are used for performing the geometric correction, were provided by the FotoTerra company.

A water surface mask was produced to exclude all non-water pixels from the images. The masks were drawn manually using ENVI 4.8. All land, macrophyte stands, boats, clouds and cloud shadows were removed, leaving only strictly open-water pixels.

2.3 Sunglint removal procedures

There are several methods available for sunglint removal from high resolution satellite images. Most methods exploit the high absorption of water at NIR wavelengths, assuming that reflectance in these bands is negligible. However, for Case II waters, NIR reflectance cannot be neglected due to TSM, and in shallow waters, NIR cannot be neglected due to bottom reflectance. We have applied three sunglint correction algorithms that allow for non-zero NIR water-leaving radiance, suitable for correcting images acquired over Case II and/or optically shallow waters. The use of NIR signals to quantify sunglint over the visible range is based on Fresnel reflectance in water bodies, which is only slightly wavelength dependent, meaning that sunglint corrections in the NIR can be similarly applied to visible wavelengths. The algorithms used in this study are described below.

2.3.1 Goodman et al. (2008) algorithm

This algorithm takes above water remote sensing reflectance, as input, which was approximated by dividing the surface reflectance values by π (MOBLEY, 1994; GOODMAN et al., 2008). The sunglint correction factor was then calculated for each pixel as a constant offset across all wavelengths, based on the difference between R_{rs} at 640 nm and 750 nm (Eq. 1 and 2):

$$R_{rs}^{deg}(\lambda) = R_{rs}^{raw}(\lambda) - R_{rs}^{raw}(750) + \Delta \quad (1)$$

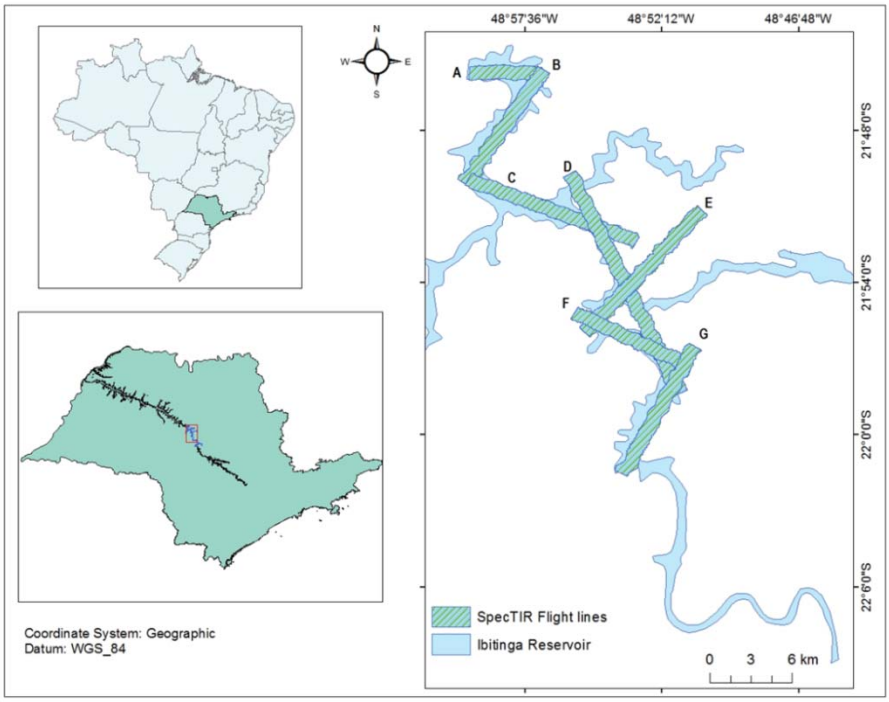

Fig. 1 - Location of Ibitinga reservoir in the state of São Paulo (Southeastern Brazil). The seven SpecTIR flight lines for the hyperspectral images are indicated by letters (A to G).

Table 1: Location and view-illumination attributes of the seven SpecTIR flight lines over Ibitinga Reservoir (São Paulo, Brazil)

Flight Line	**Starting latitude and longitude**		**Ending latitude and longitude**		**Sun Zenith angle (º)**	**Sun Azimuth angle (º)**
	S	*W*	*S*	*W*		
A	21°45'40.92"	48°59'49.13"	21°45'43.09"	48°57'1.61"	52.7	88.3
B	21°50'5.32"	48°59'59.04"	21°45'32.39"	48°56'50.44"	50.4	87.2
C	21°49'54.67"	48°59'52.39"	21°52'19.84"	48°53'16.24"	37.9	80.7
D	21°49'45.31"	48°55'47.96"	21°58'22.09"	48°51'28.89"	35.6	79.4
E	21°55'56.98"	48°55'13.14"	21°51'8.04"	48°50'38.77"	39.9	82.0
F	21°55'10.78"	48°55'38.73"	21°57'10.09"	48°51'20.91"	33.7	77.9
G	22°1'32.00"	48°53'44.36"	21°56'31.70"	48°50'54.29"	31.7	76.3

$$\Delta = 0.000019 + 0.1[R_{rs}^{raw}(640) - R_{rs}^{raw}(750)] \quad (2)$$

where is the deglinted remote sensing reflectance at each wavelength; is the raw above water remote sensing reflectance at each wavelength; is the raw above water remote sensing reflectance at 750 nm; is the raw above water remote sensing reflectance at 640 nm, and is the offset added to each wavelength. The constants 0.000019 and 0.1 are given by Lee et al. (1999). According to them, these values can be applied to images obtained by any hyperspectral sensor that has bands located at 750 nm and 640 nm.

After sunglint correction, the resulting images (deglinted images) were converted back to surface reflectance to facilitate interpretation of the results.

2.3.2 Kutser et al. (2009) algorithm

This method uses information from the oxygen absorption band located around 760 nm, assuming that the amount of sunglint is proportional to the depth of the oxygen absorption feature (*OD)*. In the present study, because the sensor does not include a band at 760 nm, we selected the band centered at 753

nm for the calculations (Eq. 3):

$$OD = \frac{R_{rs}^{raw}(738) + R_{rs}^{raw}(860)}{2} - R_{rs}^{raw}(753) \quad (3)$$

where *OD* is the oxygen absorption depth, and , and are the raw reflectance values at each of these wavelengths.

Since the bands at 738 nm and 860 nm comprise the shoulders of the oxygen absorption band, the average of their reflectance values gives an estimate of the expected reflectance in the absence of oxygen. When *OD* is zero, the pixel can be assumed to have no sunglint. For each pixel, *OD* is normalized by dividing it by the maximum *OD* observed for a deep water region, *i.e.* the maximum sunglint value OD_{max} (Eq. 4):

$$OD_{norm}(x,y) = \frac{OD(x,y)}{ODmax} \quad (4)$$

The spectral variation of sunglint *G(λ)* is then calculated by subtracting the spectrum at the darkest (i.e., lowest *OD*) NIR deep-water pixel from the brightest (Eq. 5):

$$G(\lambda) = S(bright) - S(dark) \quad (5)$$

The product of *G*(λ) and the normalized depth (OD_{norm}) gives the amount of sunglint for each band at each pixel. This amount can then be subtracted from the uncorrected reflectance to give the corrected water-leaving reflectance *Rdeglint* (Eq. 6):

$$Rdeglint\ (x,y,\lambda) = R(x,y,\lambda) - G(\lambda) * OD_{norm}(x,y) \quad (6)$$

2.3.3 Modified Kutser et al. (2009) algorithm

A variant of the KUTSER et al. (2009) method was also tested in our analysis, where instead of using Equation 3, we calculated the depth of the oxygen absorption band using the continuum removal technique described by CLARK & ROUSH (1984). The continuum is a straight line fitted over the top of a spectrum that connect local spectral maxima and represents the "background absorption" onto which other absorption features are superimposed (CLARK, 1999). The continuum is removed by dividing the reflectance value for each point in the absorption feature by the reflectance level of the continuum line at the corresponding wavelength. Therefore, the main difference between the two methods (KUTSER et al., 2009 and its variant) was a function only of how the OD values were obtained.

In order to define the straight line, we selected the same wavelengths of Equation 3 (738 nm and 860 nm) as the starting and ending points and then removed the continuum (Eq. 7):

$$R_{cr}(\lambda) = \frac{R_{original}(\lambda)}{R_{continuum}(\lambda)} \quad (7)$$

where is the normalized reflectance after the continuum removal; is the surface reflectance at a given wavelength; and is the surface reflectance projected onto the straight line at the same wavelength.

The resulting continuum removal image was then used to calculate the oxygen absorption band depth (OD_{pb}) (Eq. 8):

$$OD_{pb} = 1 - R_{cr}\ (753nm) \quad (8)$$

The remaining procedures were the same as those described for the original Kutser et al. (2009) method to obtain the final image.

2.4 Relative assessment of the sunglint methods in the study area

From the total set of seven SpecTIR images, we selected two highly sunglint affected scenes (D and G in Fig. 1) to evaluate the relative performance of the GOODMAN et al. (2008), KUTSER et al. (2009) and the modified KUTSER et al. (2009) methods.

Two different approaches were used for this purpose. First, the difference between reflectance values in sunglint contaminated and deglinted images was calculated for each method, resulting in residual reflectance images. Residual values were then grouped into categorical intervals, which accounted for different classes of sunglint intensities. The best method for sunglint removal was assumed to be the one consistently with the largest residual reflectance values.

In the second approach, homogeneous water masses partially affected by sunglint were manually delineated using field information (acquired simultaneous to image acquisition) and visual inspection of true color composites (Fig. 2a) to verify the consistency of results from the first approach. Assuming similar concentrations of OAS in these water masses, any substantial

changes in pixel reflectance spectra observed in these areas could be attributed mainly to sunglint effects. After defining homogeneous water masses, spatial transects were traced across each region from the non-affected areas to the portions of the scene under the largest sunglint influence (Fig. 2b). Reflectance profiles were extracted from each transect for three bands in the VIS (460, 548, 638 nm) and two bands in the NIR (782 nm and 860 nm). For each profile, reflectance values before and after the application of each method were compared.

To ensure confidence in the analysis and to take into account possible variations caused by factors such as SNR, we also calculated average reflectance differences for regions of interest (ROIs) with size of 30 x 30 pixels within the non-affected and affected sunglint areas of each water mass (Fig. 2c). Five pairs of samples (ROIs) were used in this analysis: two on scene G (G1 and G2) and three on scene D (D1, D2 and D3). The method that had the lowest amplitude of reflectance values between homogenous water masses affected and non-affected by sunglint was considered the best correction methodology.

3. RESULTS AND DISCUSSION

Overall, results indicated that the algorithms tested had variable efficiency in removing sunglint effects from high resolution hyperspectral imagery. The results also provided a better understanding of sunglint patterns and magnitudes across each image. We present the results of the comparative evaluation below, and discuss the relative performance and limitations of each method.

3.1 Sunglint effects on SpecTIR images

Sunglint occurred predominantly in the eastern edges of the five scenes (B, D to G) acquired with a flight direction of less than 270° (Fig. 3), and on the northern edges of two scenes (A and C) obtained with flight directions of 296° and 300°, respectively. The Sun was positioned east from the sensor in every acquired scene. This pattern of increasing brightness towards the image edges is characteristic of cross-track sunglint, and has been similarly observed in Airborne Visible InfraRed Imaging Spectroradiometer (AVIRIS) images (MUSTARD et al., 2001; GOODMAN et al., 2008), as well as in SpecTIR images (MILLER, 2012; BURT, 2012).

Cross-track glint occurs when the sun angle is such that sunglint manifests itself perpendicular to the motion of the sensor (MILLER, 2012). It results in higher brightness values for half the image, from nadir towards one edge of the scene, while the remaining half has little or no sunglint effects. When scanning along the FOV, changes in aircraft attitude (position) result in different instantaneous viewing zenith angles relative to the surface, which can enhance reflectivity of non-Lambertian targets when illumination angles approach the viewing angles. This is particularly important when assessing the spatial distribution of the sunglint, as edge pixels tend to saturate and prevent the acquisition of water radiometric information in these areas.

Although SpecTIR sensor has a relatively narrow FOV (24°), the effects of cross-track sunglint were still apparent (Fig. 3). In the images acquired over Ibitinga reservoir, an increase of up to 3% in the reflectance values were caused by sunglint effects. These results were in agreement with values reported by KAY et al. (2009) and PARK et al. (2010) in which sunglint increased reflectance values by a factor of up to 2.

3.2 Evaluation of sunglint removal methods

The analysis of residual reflectance images showed that the GOODMAN et al. (2008) algorithm removed larger amounts of sunglint when compared with the other two methods (Fig. 4a). The KUTSER et al. (2009) and the modified KUTSER et al. (2009) methods had similar performances but resulted in lower residual reflectance values than the GOODMAN et al. (2008) algorithm (Figs. 4b and 4c).

Both the original and the modified versions of the KUTSER et al. (2009) method required a laborious refinement of the land mask to eliminate all possible floating macrophyte stands in the images. Macrophytes have a much stronger radiance signal than open water, which in turn severely bias the calculation of D_{norm} and results in compression of the remaining reflectance values within the radiometric scale. Given its formulation, the GOODMAN et al. (2008) method was significantly more resilient to this type of signal contamination.

Transect analysis over homogenous water

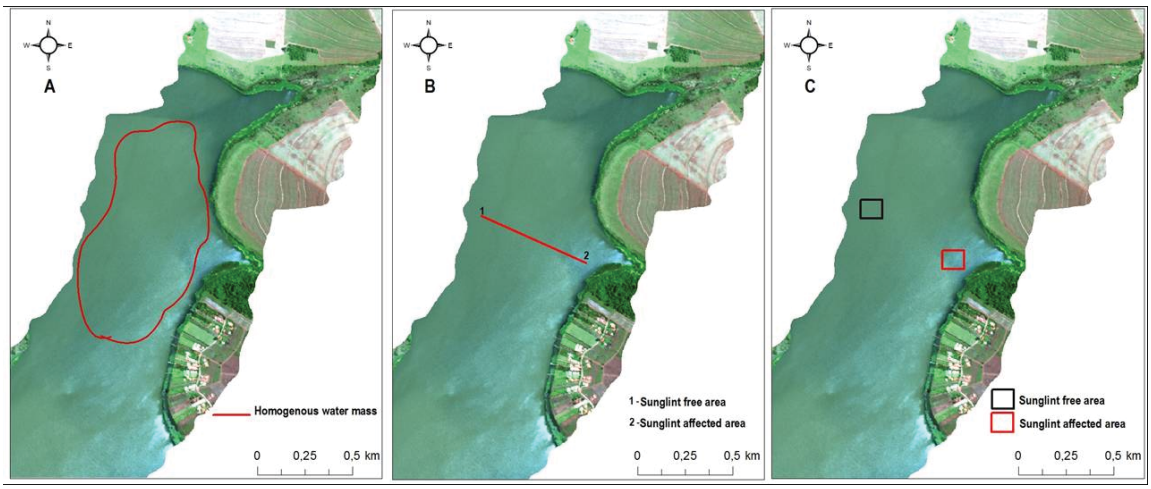

Fig.2 - True color composites using SpecTIR bands at 638 nm (red), 548 nm (green) and 460 nm (blue) showing: (a) a homogeneous water mass partially affected by sunglint; (b) a transect from which reflectance profiles were extracted; and (c) an example pair of ROIs (30 x 30 pixels) for extraction of reflectance values of non-affected (black square) and affected (red one) sunglint areas.

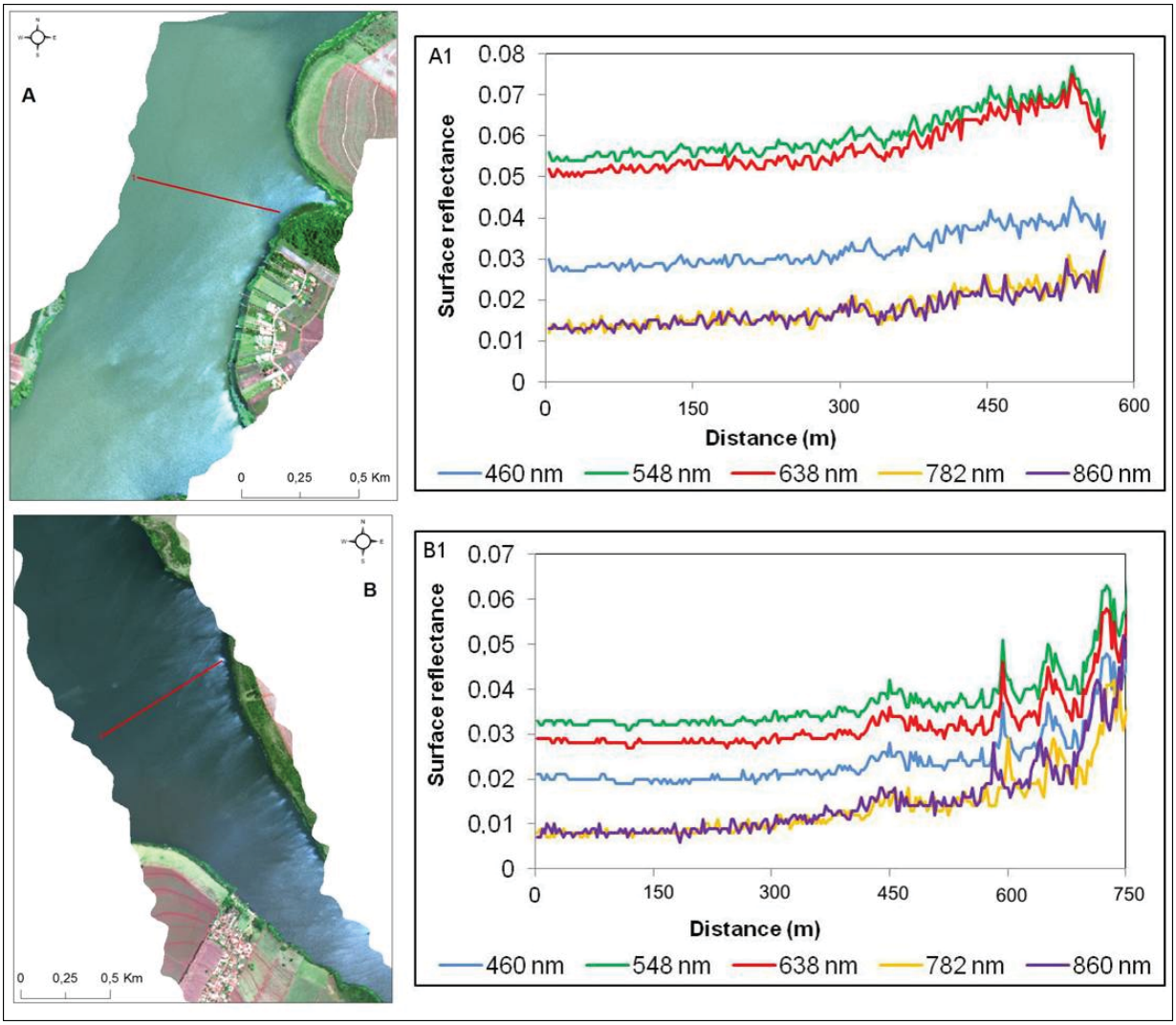

Fig. 3 - Examples of sunglint occurrence in SpecTIR hyperspectral images acquired over Ibitinga reservoir (São Paulo, Brazil). In (a) and (b), subsets of homogeneous waters masses affected by sunglint on the eastern side of the scenes are shown] for scenes G and D, respectively. Variations in reflectance of selected SpecTIR bands for transects (red lines) indicated in the images are shown at the right portion of the figures. The bands used in the true color composites are the same as in Fig. 2.

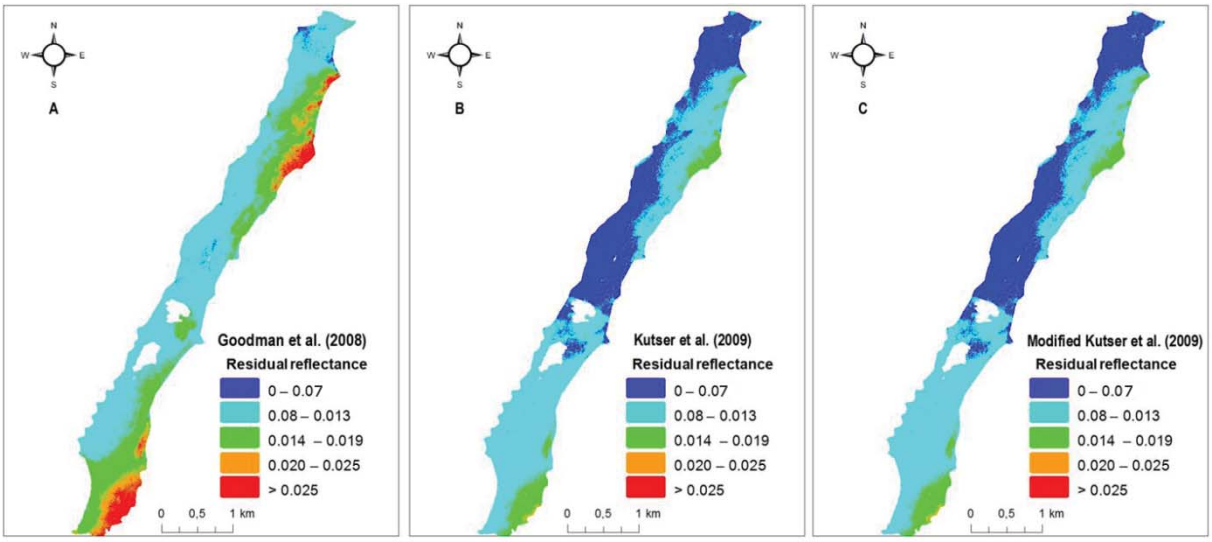

Fig. 4 - Density slice of the residual SpecTIR reflectance images over the Ibitinga reservoir after sunglint correction using the methods by: (a) GOODMAN et al. (2008); (b) KUTSER et al. (2009); and (c) modified KUTSER et al. (2009).

masses showed that images corrected by the GOODMAN et al. (2008) method presented the best results (Fig. 5a), resulting in deglint reflectance profiles with greater similarity along the transects. Images corrected using the original and the modified KUTSER et al. (2009) algorithms had residual sunglint, especially in the most affected portions of the scenes (Figs. 5b and 5c), as indicated by increasing reflectance values from the left to the right side of the transects. These results agreed with those obtained by MILLER (2012), who also observed residual sunglint effects after using the KUTSER et al. (2009) method in a SpecTIR image of a coastal zone.

Although the modified KUTSER et al. (2009) method had a similar performance when compared to its original version for scene G, the method was too sensitive to noisy data for other scenes. This most likely occurred due to either variation in instrumental SNR or to artifacts generated from atmospheric correction that introduced variability in the calculation of the oxygen absorption band depth using the continuum removal approach.

The quantitative comparison between non-affected (sunglint-free) and sunglint-affected ROI samples corroborated the results from the transect analysis. The best performance was obtained by the GOODMAN et al. (2008) algorithm, which was capable of reducing the differences between averages reflectance to values very close to zero (Table 2). Both the original and the modified versions of the KUTSER et al. (2009) method resulted in larger differences between the means of the ROIs, with variable results among specific wavelengths. Furthermore, the original KUTSER et al. (2009) method overcorrected sunglint effects on sample G1, as highlighted by the negative differences (Table 2).

4. CONCLUSIONS

Sunglint affected the radiometric quality of the high-spatial and high-spectral resolution SpecTIR images, increasing reflectance values up to 3% when compared to portions of the scenes where it was not observed. The cross-track type of sunglint was dominant in the images acquired over Ibitinga reservoir, especially towards the image edges positioned at the same side as the Sun.

The sunglint correction algorithm proposed by GOODMAN et al. (2008) presented the best results when compared to the two other tested methods, showing the lowest reflectance differences between sunglint-free and sunglint-affected areas for homogenous masses of waters. The KUTSER et al. (2009) method was also capable of reducing the sunglint effects, but a significant amount of residual sunglint signal remained in the most heavily affected areas of the evaluated scenes. The proposed modification of the KUTSER et al. (2009) method, based on the application of the continuum removal technique to calculate the oxygen absorption band depth,

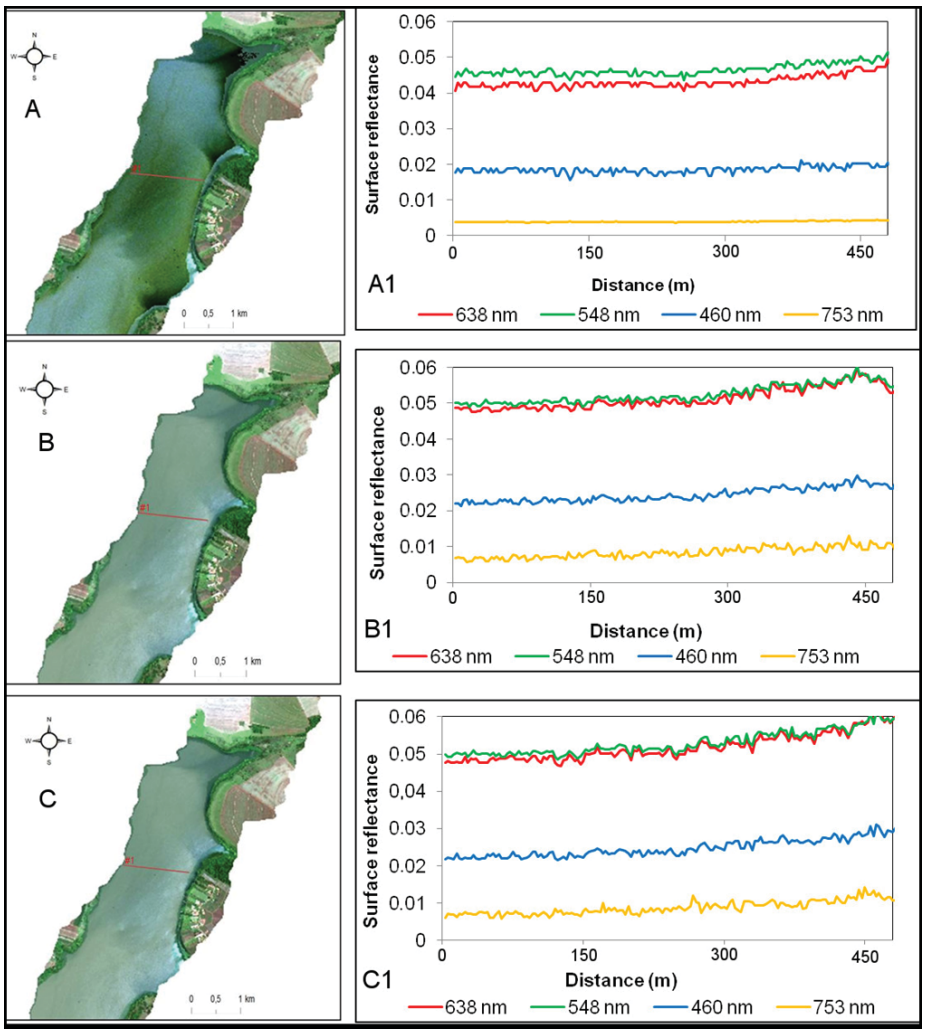

Fig. 5 - Deglinted SpecTIR hyperspectral of Ibitinga reservoir (São Paulo, Brazil) images and resultant reflectance profiles after correction by the methods of: (a) GOODMAN et al. (2008); (b) KUTSER et al. (2009); and (c) modified KUTSER et al. (2009). The bands used in the SpecTIR true color composites are the same as in Fig. 2.

also had good results. However, its performance was strongly scene dependent due to artifacts generated from atmospheric correction around this feature and to instrumental SNR.

ACKNOWLEDGMENTS

The authors thank CAPES fellowship supporting Ms. Streher, obtained through the Remote Sensing Post-Graduate Program at INPE, where this research took place. The authors also thank FAPESP for funding the image acquisition through the BIOEN program (08/56252-0) and for the financial support for Dr. Silva (2010/11269-2). We thank FotoTerra for providing the images and to Jürgen Langenwalter for the help in interpreting image metadata parameters.

Table 2: Differences in average reflectance at five specific wavelengths (λ) between sunglint-free and sunglint-affected samples from homogeneous water masses in SpecTIR hyperspectral images of Ibitinga reservoir

		Reflectance Differences			
ROI	**λ**	**Original Scene**	**Goodman**	**Kutser**	**Kutser mod.**
D1	460 nm	0.0293	-0.0072	0.0137	0.0198
	548 nm	0.0328	-0.0036	0.0133	0.0242
	638 nm	0.0342	-0.0022	0.0161	0.0231
	753 nm	0.0362	-0.0002	0.0194	0.0230
	860 nm	0.0347	-0.0018	0.0190	0.0222
D2	460 nm	0.0236	-0.0052	0.0267	0.0193
	548 nm	0.0253	-0.0042	0.0084	0.0243
	638 nm	0.0273	-0.0022	0.0124	0.0286
	753 nm	0.0295	-0.0002	0.0144	0.0290
	860 nm	0.0275	-0.0022	0.0122	0.0259
D3	460 nm	0.0152	-0.0072	0.0054	-0.0122
	548 nm	0.0173	-0.0051	0.0055	-0.1248
	638 nm	0.0181	-0.0042	0.0078	-0.1154
	753 nm	0.0220	-0.0003	0.0114	0.1251
	860 nm	0.0215	-0.0009	0.0113	0.1338
G1	460 nm	0.0147	-0.0049	-0.2303	0.0076
	548 nm	0.0109	-0.0088	-0.5544	0.0006
	638 nm	0.0058	-0.0138	-0.3918	0.0026
	753 nm	0.0184	-0.0012	-0.0498	0.0097
	860 nm	0.0182	-0.0014	-0.0513	0.0086
G2	460 nm	0.0123	-0.0020	0.0073	0.0524
	548 nm	0.0145	0.0002	0.0102	0.0492
	638 nm	0.0170	0.0028	0.0131	0.0626
	753 nm	0.0145	0.0002	0.0078	0.0619
	860 nm	0.0136	-0.0007	0.0073	0.0587

REFERENCES

BERTELS, L.; VANDERSTRAETE, T.; VAN COILLIE, S.; KNAEPS, E.; STERCKX, S.; GOOSSENS, R.; DERONDE, B. Mapping of Coral Reefs Using Hyperspectral CASI Data; a Case Study: Fordata, Tanimbar, Indonesia. **International Journal of Remote Sensing**, v. 29, p. 2359-2391, 2008.

BURT, C. **Detection of spattially unresolved nominally sub - pixel submerged and surface targets using hyperespectral data.** 2012. Master in remote sensing intelligence - Naval Postgraduate School. Available at < http://www.dtic.mil/cgi-bin/GetTRDoc?Location=U2&doc=GetTRDoc.pdf&AD=ADA567072 > Last accessed on Jan, 02, 2013.

CASAL G., KUTSER T., DOMINGUES-GOMEZ J. A., SANCHES-CARNERO N. AND FREIRE J., Mapping benthic macroalgal communities in the coastal zone using CHRIS-PROBA mode 2 images. **Estuarine Coastal Shelf Science**, v. 94, p. 281–90, 2011.

CESP - COMPANHIA ENERGÉTICA DE SÃO PAULO, 1998. **Conservação e Manejo nos Reservatórios: Limnologia, Ictiologia e Pesca. São Paulo. Companhia Energética de São**

Paulo – Série Divulgação e Informação, 220p.

CLARK, R.N. Spectroscopy of rocks and minerals, and principles of spectroscopy *IN* A. N. Rencz Ed., **Remote sensing for the earth science** 3rd ed.. Manual of remote sensing, 3:3 – 58. New York: John Wiley and Sons, 1999.

CLARK, R.N.; ROUSH, T.L. Reflectance spectroscopy: quantitative analysis techniques for remote sensing applications. **Journal of Geophysical Research**. v. 89, n. B7, p. 6329-6340, July 10, 1984.

DEKKER, A. G.; BRANDO, V. E.; ANSTEE, J. M.; PINNEL, N.; KUTSER, T.; HOGENBOOM, H. J.; ASTERKAMP, R.; PETERS, S. W. M.; C. OLBERT, R. J. VOS.; MALTHUS, T. J. Imaging spectrometry of water**.** In:VAN DER MEER, F.; DE JONG, S. M. (Eds.). **Imaging spectrometry: basic principles and prospective applications.** Springer, Netherlands, 2001. p. 307-359.

FELDE, G.W.; ANDERSON, G.P.; ADLER-GOLDEN, S.M.; MATTHEW, N.W. & BERK, A. Analysis of Hyperion data with the FLAASH atmospheric correction algorithm. **Proceedings of the International Geoscience Remote Sensing Symposium** IGARSS, Toulouse, 21–25 July 2003, pp. 90–92. 2003.

GOODMAN, J.A.; LEE, Z.; USTIN, S.L. Influence of Atmospheric and Sea-Surface Corrections on Retrieval of Bottom Depth and Reflectance Using a Semi-Analytical Model: A Case Study in Kaneohe Bay, Hawaii. **Applied Optics**, v. 47, F1-F11, 2008.

GURLIN, D.; GITELSON, A. A. AND MOSES, W. J. Remote estimation of chl-a concentration in turbid productive waters - Return to a simple two-band NIR-red model **Remote Sensing of Environment,** v. 115**,** p. 3479-3490, 2011.

HEDLEY, J.; HARBORNE, A.; MUMBY, P. Simple and robust removal of sun glint for mapping shallow-water benthos. **International Journal of Remote Sensing**, v. 26, p. 2107-2112, 2005.

HEEDGE, T., HAUSKNECHT, P., & KOBRYN, H. Hyperspectral seafloor mapping and direct bathymetry calculation using Hymap data from the Ningaloo reef and rottnest island areas in Western Australia. In: **Proceedings of the 5th EARSel Workshop on imaging spectroscopy**, Bruges, 23–25 April, p. 1–8, 2007.

HOCHBERG, E.; ANDREFOUET, S.; TYLER, M. Sea surface correction of high spatial resolution IKONOS images to improve bottom mapping in near-shore environments**. IEEE Transactions Geosciences of Remote Sensing**., v.41, p.1724-1729, 2003.

ITT , VISUAL INFORMATION SOLUTIONS. **Atmospheric correction module: QUAC and FLAASH user's guide.** Version 4.7. Boulder: CO: ITT Visual Information Solutions. 2009.

KAY, S., HEDLEY, J.D., LAVENDER, S.. Sun glint correction of high and low spatial resolution images of aquatic scenes: a review of methods for visible and near-infrared wavelengths. **Remote Sensing,** v. 1, p. 697-730, 2009.

KEITH, D. J., DRUEKE, C., SZYKMAN, J., WUSK, M., KAGEY, L., & HOWELL, C. Trophic status , ecological condition , and cyanobacteria risk of New England lakes and ponds based on aircraft remote sensing aircraft remote sensing. **Journal of Applied Remote Sensing**, v. 6, p.1–22, 2012.

KOPONEN, S.; PULLIAINEN, J.; KALLIO, K. & HALLIKAINEN, M. Lake water quality classification with airborne hyperspectral spectrometer and simulated MERIS data. **Remote Sensing of Environment**, v.79, p.1:51-59, 2002

KUTSER, T., METSAMAA, L., STROMBECK, N., & VAHTMAE, E. Monitoring cyanobacterial blooms by satellite remote sensing. **Estuarine, Coastal and Shelf Science**, v. 67, p. 303–312. 2006.

KUTSER, T.; VAHTMÄE, E.; PAAVEL, B.; KAUER, T. Removing glint effects from field radiometry data measured in optically complex coastal and inland waters. **Remote Sensing of Environment,** v.133,p. 85-89, 2013.

KUTSER, T.; VAHTMÄE, E.; PRAKS, J.A. Sun Glint Correction Method for Hyperspectral Imagery Containing Areas with Non-Negligible Water Leaving NIR Signal. **Remote Sensing of Environment**,**.** v. 113, p. 2267-2274, 2009.

LEE Z., CARDER, K. MOBLEY, C. D., STEWARD, R. AND PATCH J.. Hyperspectral

remote sensing for shallow waters: 2. Deriving bottom depths and water properties by optimization. **Applied Optics**, v. 38**, p.** 3831-3843, 1999.

LYZENGA, D.; MALINAS, N.; TANIS, F. Multispectral Bathymetry Using a Simple Physically Based Algorithm. **IEEE Transactions Geosciences of Remote Sensing**. v. 44, p. 2251-2259, 2006.

MILLER, C. **Evaluation of sun glint correction algorithms for high-spatial resolution hyperspectral imagery**. 2012. Master in remote sensing intelligence - Naval Postgraduate School < http://hdl.handle.net/10945/17421> Last accessed on Jan, 02, 2013.

MOBLEY, C.D. **The optical properties of water**. New York: McGraw-Hill Book, 1994, 592p.

MOREL, A.; PRIEUR, L. Analysis of variations in ocean colour. **Limnology and Oceanography**, v. 22, n. 4, p. 709-722, 1977.

MOSES, W. J., A.A. GITELSON, R. L. PERK, D. GURLIN, D. C. RUNDQUIST, B. C. LEAVITT, T. M. BARROW, & BRAKHAGE, P.. Estimation of chlorophyll-a concentration in turbid productive waters using airborne hyperspectral data. **Water research**, v. 46, n. 4, p. 993-1004, 2012.

MUSTARD, J.; STAID, M.; FRIPP, W. A semianalytical approach to the calibration of AVIRIS data to reflectance over water application in a temperate estuary. **Remote Sensing of Environment**, v.75, p.335-349, 2001.

ODERMATT, D., GITELSON, A., BRANDO, V. E., & SCHAEPMAN, M.. Review of constituent retrieval in optically deep and complex waters from satellite imagery. **Remote sensing of environment**, v. 118, p. 116-126, 2012.

OLMANSON, L. G.; BREZONIK, P. L. AND BAUER, M.E. Airborne hyperspectral remote sensing to assess spatial distribution of water quality characteristics in large rivers: The Mississippi River and its tributaries in Minnesota. **Remote Sensing of Environment,** v.130, p. 254-265, 2013.

PARK, Y., DEKKER, A., & HOCHBERG, E. Glint-aerosol discrimination using NIR-SWIR wavelengths. In: **HyspIRI Sun Glint Report**

HyspIRI Science Workshop, 24-26 Aug, **,** JPL Publication 11-4**,** 2010.

SILVA, T.S.F.; COSTA, M.P.F.; MELACK, J.M.; NOVO, E.M.L.M. Remote sensing of aquatic vegetation: theory and applications. **Environment Monitoring Assessment**, v.140**, p.**131–45, 2008.

VOSS, K. J.; MOREL, A. Bidirectional reflectance function for oceanic waters with varying chlorophyll concentrations: Measurements versus predictions. **Limnology and Oceanography**, v.50, no. 2 698-705, 2005.